Characterization of the Drug Binding Specificity of Rat Liver Fatty Acid Binding Protein

Sara Chuang,[†] Tony Velkov,[†] James Horne,[†] Christopher J. H. Porter,*[,‡] and Martin J. Scanlon*[,†]

Medicinal Chemistry and Drug Action, Monash Institute of Pharmaceutical Sciences, Monash University (Parkville Campus), 381 Royal Parade, Parkville 3052 Victoria Australia, Drug Delivery, Disposition and Dynamics, Monash Institute of Pharmaceutical Sciences, Monash University (Parkville Campus), 381 Royal Parade, Parkville 3052 Victoria Australia

Received September 23, 2007

Liver-fatty acid binding protein (L-FABP) is found in high levels in enterocytes and is involved in the cytosolic solubilization of fatty acids during fat absorption. In the current studies, the interaction of L-FABP with a range of lipophilic drugs has been evaluated to explore the potential for L-FABP to provide an analogous function during the absorption of lipophilic drugs. Binding affinity for L-FABP was assessed by displacement of a fluorescent marker, 1-anilinonaphthalene-8-sulfonic acid (ANS), and the binding site location was determined via nuclear magnetic resonance chemical shift perturbation studies. It was found that the majority of drugs bound to L-FABP at two sites, with the internal site generally having a higher affinity for the compounds tested. Furthermore, in contrast to the interaction of L-FABP with fatty acids, it was demonstrated that a terminal carboxylate is not required for specific binding of lipophilic drugs at the internal site of L-FABP.

Intracellular lipid binding proteins (iLBPs) are a family of phylogenetically related low molecular weight proteins. Although various functions have been proposed for iLBPs, it is widely accepted that they bind to poorly water soluble ligands in the cytosol, thereby facilitating improved intracellular solubilization.[1,2] Several classes of iLBPs have been isolated, including sterol carrier proteins, retinol binding proteins, and fatty acid binding proteins (FABPs),[a2,3] all of which display similar tertiary structures. The iLBP fold contains 10 antiparallel β-strands that form a clam-shell-like structure, capped by a pair of α-helices[4] (Figure 1). The iLBPs are further categorized into four major subfamilies on the basis of sequence homology and ligand binding characteristics.[4] Subfamily I comprises proteins with specific affinity for vitamin A derivatives, subfamily II contains proteins with larger binding cavities and includes L-FABP, subfamily III consist only of intestinal fatty acid binding protein (I-FABP), and subfamily IV is characterized by an additional α-helical loop at the N-terminus.[1,4] The absorptive cells that line the small intestine (enterocytes) contain high levels of two iLBPs, liver and intestinal fatty acid binding protein (L-FABP and I-FABP). L-FABP and I-FABP constitute up to 5%[5,6] and 3% of total cytosolic protein,[7] respectively. The FABPs bind to different lipids with varying affinity and specificity.[8] Numerous functions have been suggested for iLBPs, including modulation of enzyme activity, signal transduction, control of differentiation and growth regulation as well as intracellular transport and storage of fatty acids,[9] however, the relative importance of their functionality remains unclear.[10] During the absorption of dietary lipids, the enterocyte is exposed to high concentrations of fatty acid (FA), and I- and L-FABP have been suggested to bind fatty acids within the cytosol, thereby facilitating intracellular transport and reducing cellular exposure to high (and potentially toxic) concentrations of free FA.[11] However, even during lipid absorption, the relative intracellular concentrations of FABP and FA suggest that significant quantities of apo-FABP are present in the cell cytoplasm.[12,13] This raises the possibility that FABPs may play a role in the intracellular transport of other (exogenous) molecules. In this regard, it has been demonstrated that I-FABP is able to bind to several classes of lipophilic drugs,[13,14] and in a model membrane system, I-FABP has been shown to facilitate the transmembrane transport of these drugs.[15] L-FABP is present in the enterocyte at higher concentrations than I-FABP and typically shows much broader binding specificity for endogenous ligands. L-FABP possesses a larger binding cavity than I-FABP and is capable of binding two FA molecules, whereas I-FABP binds only a single FA.[16–18] Together these data suggest that L-FABP may also have a role in the transport of poorly water soluble drugs.

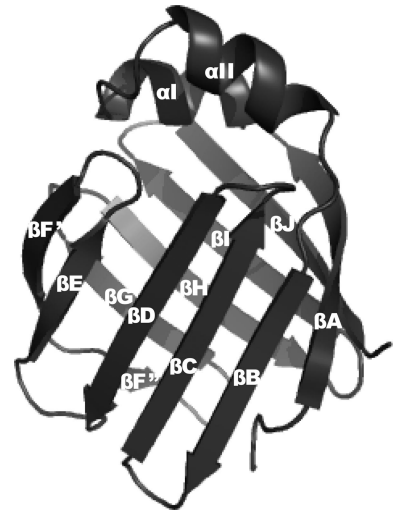

Figure 1. Ribbon diagram of the X-ray crystal structure of L-FABP (Protein Data Bank ID 1LFO). Strands βA−βJ and helices αI−αII are labeled. This illustration was prepared with the use of PyMol v0.99.

* To whom correspondence should be addressed. Phone: +61 3 9903 9540 or +61 3 9903 9649. Fax: +61 3 9903 9582. E-mail: Martin.Scanlon@vcp.monash.edu.au (M.J.S.); Chris.Porter@vcp.monash.edu.au (C.J.H.P.).

[†] Medicinal Chemistry and Drug Action, Monash Institute of Pharmaceutical Sciences.

[‡] Drug Delivery, Disposition and Dynamics, Monash Institute of Pharmaceutical Sciences.

[a] Abbreviations: FABP, fatty acid binding protein; L-FABP, liver fatty acid binding protein; I-FABP, intestinal fatty acid binding protein; FA, fatty acid; OLA, oleic acid; ANS, 1-anilinonaphthalene-8-sulfonic acid; DMSO, dimethylsulfoxide.

10.1021/jm701192w CCC: $40.75
Published on Web 06/06/2008

Although structurally similar, differences between I-FABP and L-FABP have resulted in different iLBP subfamily classification. I-FABP is unique in both sequence and ligand binding characteristics and is the only member of subfamily III of the iLBPs. I-FABP binds a single FA molecule in a slightly bent conformation, with the carboxylate headgroup buried within the cavity and the methylene tail extending toward the helical region.[4] L-FABP falls into iLBP subfamily II, the members of which have a characteristically larger binding cavity. For example, L-FABP has a binding cavity of 610 Å^2, which is almost double that I-FABP (353 Å^2).[2] This allows for the binding of bulkier ligands such as bile acids, eicosanoids, and heme.[1] The larger binding cavity also enables L-FABP to bind fatty acids at a stoichiometric ratio of 1:2. The first FA molecule is fully enclosed within the barrel structure of the protein in a bent conformation, and the carboxylate group interacts with a positively charged arginine residue, deep within the binding pocket. The second FA binds "tail first" with the carboxylate group protruding from the protein.[9] The second FA consequently binds mainly via hydrophobic forces. While L-FABP is known to bind to fatty acids with high affinity, it has also been found to bind to a range of other compounds, including bile salts, bilirubin, lysophosolipids, cyclopentenone, and other hydrophobic compounds such as fibrates.[2,9,11]

The high abundance of L-FABP in enterocytes, in conjunction with its broad binding specificity, suggests that it may also be involved in the cytosolic solubilization and transport of a range of lipophilic molecules. In this study, we have determined the binding affinity of L-FABP for a range of lipophilic drugs and characterized their modes of binding. The binding specificity of L-FABP has been examined using a competitive fluorescence displacement assay, and binding site locations have been investigated by NMR. These studies suggest a potential role for L-FABP in intracellular transport and cellular disposition of a range of lipophilic drugs.

Experimental Procedures

Materials. Potential ligands for L-FABP are shown in Figure 3 and were obtained from Sigma-Aldrich (Sydney, N.S.W., Australia). Isopropyl β-D-thiogalactopyranoside was purchased from Merck (Victoria, Australia). *Escherichia coli* strain BL21 Codon Plus (DE3)-RIL was purchased from Stratagene (La Jolla, CA). All other reagents were of the highest purity available commercially.

Expression and Purification of Rat L-FABP. Recombinant L-FABP was expressed in BL21(DE3)/pTrc99A host/vector expression system as described previously.[19] Briefly, the cells were grown in Luria−Bertani or ^{15}N-labeled minimal media containing ampicillin (100 μg/mL) before induction with IPTG (1 mM). Cells were harvested by centrifugation (4000*g* for 30 min at 4 °C) 4 h post induction. The pellets were resuspended in buffer A (50 mM Tris-HCl, pH 8.0, 150 mM NaCl, 1 mM DTT, 0.5 mM EDTA) and lysed by sonication. The resulting homogenate was clarified by centrifugation (12000*g* for 30 min at 4 °C). Ammonium sulfate was added to the supernatant to 60% saturation, and the soluble fraction was recovered by centrifugation (20000*g* for 20 min at 4 °C). Ammonium sulfate was removed via application to a Phenyl HP 16/10 column (Amersham Biosciences, N.S.W., Australia). L-FABP was eluted with a linear gradient from 100−0% 1.0 M $(NH_4)_2SO_4$ over 1 column volume, and fractions containing L-FABP were detected by SDS-PAGE. Nucleic acids were removed by addition of protamine sulfate (0.1% w/v). Protein solution was buffer exchanged into buffer A and applied to a MonoQ HR 10/10 column (Amersham Biosciences, N.S.W., Australia) in the same buffer. L-FABP was eluted in the unbound fraction. L-FABP containing fractions were exchanged into buffer B (50 mM Tris-HCl, pH 8.0, 1.0 M $(NH_4)_2SO_4$, 1 mM DTT, 0.5 mM EDTA) and applied to a Phenyl HP 16/10 column. L-FABP was eluted with a linear gradient from 100−0% 1.0 M $(NH_4)_2SO_4$ over 1 column volume, and fractions containing L-FABP were detected by SDS-PAGE. The Phenyl HP column efficiently delipidated L-FABP. Delipidation was confirmed by mass spectrometry of ethyl acetate extracts of purified protein, which revealed that lipids had been removed. Fractions containing L-FABP were pooled, buffer exchanged, and concentrated by ultrafiltration. Homogeneity of the purified protein was assessed by SDS-PAGE, and purity was characterized by electrospray ionization mass spectrometry on a Micromass Platform II liquid chromatography/quadrupole mass spectrometry system (Manchester, UK). Protein concentration was determined by UV−visible spectrophotometry using a molar extinction coefficient at 280 nm of 6400 (cm M)$^{-1}$.

Fluorescence Measurements. Steady-state fluorescence spectra were measured on a Cary Eclipse fluorescence spectrophotometer equipped with a 4 cell block temperature controller (Varian, Mulgrave, Victoria, Australia) using a 1 cm path length cuvette. The binding of L-FABP to the fluorescent probe, ANS, was monitored by measuring the fluorescence signal between 450 and 550 nm following excitation at 400 nm. Slit widths were set to 5 and 10 nm for the excitation and emission monochromators, respectively. To assess its binding affinity for L-FABP, ANS (0−70 μM) was titrated into a solution of L-FABP (1 μM in 1 mL buffer C-20 mM MES, pH 5.5, 100 mM NaCl, 1 mM DTT, 0.5 mM EDTA). The concentration of ANS was quantified by UV−visible spectrophotometry using a molar extinction coefficient at 350 nm of 4950 (cm M)$^{-1}$. All measurements were performed at 20 °C, and samples were equilibrated for 2 min prior to measurement.

Data modeling operations were performed with GraphPad Prism version 4.0 software (GraphPad Software, San Diego, CA). ANS fluorescence, corrected for dilution, was fitted to both a one-site binding hyperbola (eq 1) and a two-site binding hyperbola (eq 2).

$$\Delta F = F_{max} \times [ANS]/(K_d + [ANS]) \quad (1)$$

$$\Delta F = F_{max1} \times [ANS]/(K_{d1} + [ANS]) + F_{max2} \times [ANS]/(K_{d2} + [ANS]) \quad (2)$$

ΔF is the enhancement in fluorescence intensity upon binding of ANS to L-FABP to a point of maximum enhancement (F_{max}).

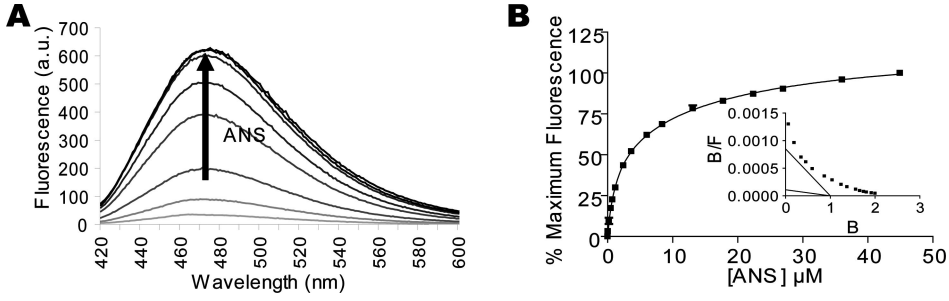

Figure 2. (A) Fluorescence emission spectra for a solution of L-FABP in the presence of increasing concentrations of ANS. The arrow indicates the direction of increasing ANS concentration. (B) ANS binding curve of L-FABP obtained from the fluorescence titrations. The solid line represents the best fit to the two-site binding hyperbola. Inset: Scatchard plot of ANS binding data for L-FABP where B/F represent bound/free and B represents bound. The ANS binding curve appear to saturate at approximately 2 ANS bound per L-FABP.

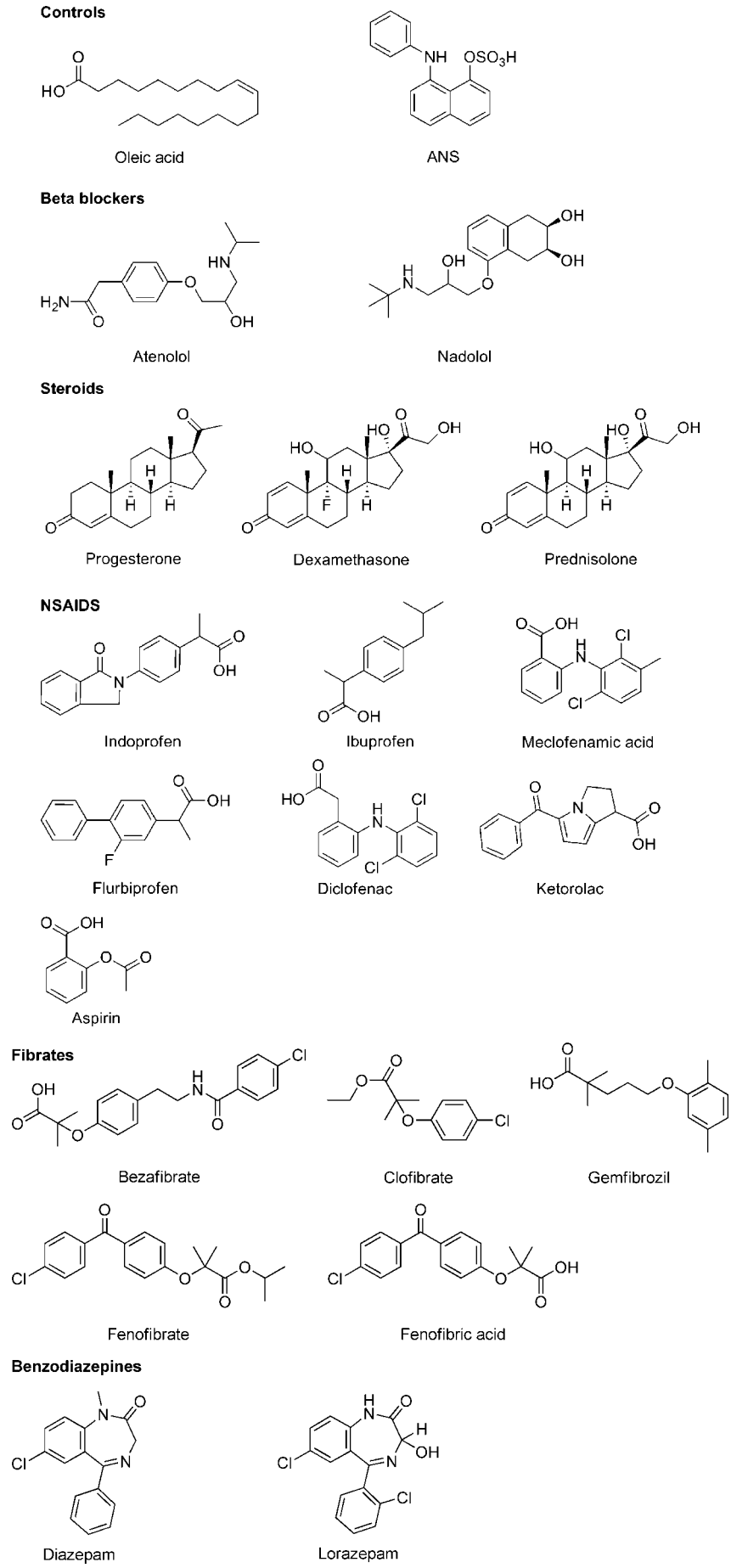

Figure 3. Chemical structures of drugs examined for L-FABP binding affinity.

Statistical comparisons between one-site and two-site binding hyperbolas were made using extra-sum-of-squares *F*-test with GraphPad Prism version 4.0 software (GraphPad Software, San Diego, CA). The one-site binding hyperbola was rejected when $p < 0.05$ and data fit to the two-site binding hyperbola.

Where binding was determined to fit the two-site binding hyperbola, data were fit to the Hill equation (eq 3) to determine an apparent dissociation constant and the degree of cooperativity using the Hill constant, *n*.

$$\Delta F = [\mathrm{ANS}]^n/(K_d + [\mathrm{ANS}]^n) \quad (3)$$

Drug binding to L-FABP was measured by recording the change in fluorescence upon displacement of ANS. Displacement data were obtained using L-FABP (1 μM in 1 mL of Buffer C) with a saturating quantity of ANS (70 μM). Freshly prepared drug solutions in dimethylsulfoxide (DMSO) were titrated into the L-FABP-ANS sample. Displacement was measured as a decrease of fluorescence signal between 450 and 550 nm following excitation at 400 nm. Fluorescence signals were corrected for dilution, and DMSO concentration was kept below 10% (v/v). Titration with 10% (v/v) DMSO in buffer C alone produced no significant changes in fluorescence of ANS. Displacement data were fit to one-site competition (eq 4) and two-site competition models (eq 5) and compared. The one-site competition model was rejected when $p < 0.05$ and data fit to the two-site competition model.

$$\Delta F = \{[\mathrm{ANS}] \times F_{max}/([\mathrm{ANS}]+K_d)\times(1 + [\mathrm{Ligand}]/K_i)\} + \mathrm{NS} \quad (4)$$

$$\Delta F = \mathrm{SITE1} + \mathrm{SITE2} + \mathrm{NS}$$
$$\mathrm{SITE1} = [\mathrm{ANS}] \times F_{max1}/([\mathrm{ANS}] + K_{d1} \times (1 + [\mathrm{Ligand}]/K_{i1}))$$
$$\mathrm{SITE2} = [\mathrm{ANS}] \times F_{max2}/([\mathrm{ANS}] + K_{d2} \times (1 + [\mathrm{Ligand}]/K_{i2})) \quad (5)$$

Nonspecific binding is denoted NS. SITE1 represents the high affinity binding site of L-FABP, K_{d1} and F_{max1} relates to the binding constant of ANS and maximal fluorescence induced by the ANS binding, respectively, as determined from eq 2. SITE2 represents the low affinity binding site of L-FABP, K_{d2} and F_{max2} relates to the binding constant of ANS and maximal fluorescence induced by the ANS binding, respectively, as determined from eq 2. These equations also allow the determination of inhibition constant (K_i) for each ligand at each binding site.

NMR Spectroscopy. NMR experiments were carried out on Varian Unity Inova 600 MHz spectrometer equipped with a single axis gradient triple resonance cryoprobe. Two-dimensional $^1H-^{15}N$ heteronuclear single-quantum correlation (2D $^1H-^{15}N$ HSQC) spectra were recorded on a sample of ^{15}N-L-FABP (100 μM in buffer C prepared in 95% H_2O, 5% D_2O) at 22 °C, with 1024 points and 128 increments. Data were processed using NMRPipe.[20] The data were multiplied by Gaussian and shifted-sine bell windows in ^1H and ^{15}N, respectively, and zero-filled to 2048 × 1024 points. Spectra were analyzed using the program SPARKY.[21] Titrations were performed by adding microliter amounts of each test compound to the ^{15}N labeled sample. The sample was mixed and allowed to equilibrate prior to ^{15}N-HSQC data collection. Test compounds were prepared in either buffer C or DMSO. Titration of up to 10% (v/v) DMSO into the protein produced no significant chemical shift perturbations.

Overall weighted average chemical shift changes (Δavg) were calculated for all residues using the equation:[22]

$$\Delta\mathrm{avg} = (((\delta H)^2 + (\delta N \times 0.154)^2)/2)^{0.5} \quad (6)$$

Residues that underwent the greatest changes in chemical shift were mapped onto the crystal structure of L-FABP (1LFO).[18] Significant changes were defined as more than one standard deviation greater than the mean change.

Molecular Docking. Docking calculations were performed using Glide V4.0[23] as implemented by Maestro V7.5 (Schrödinger L.L.C., New York). The crystal structure of oleate bound-L-FABP (1LFO), and molecules used for docking (ANS, ibuprofen, ketorolac, progesterone, and oleic acid) were prepared following the recommended protocol within Glide. Bound oleates and structured water molecules were ignored during docking in the high affinity binding site; however, the oleate in the high affinity site of the crystal structure was retained for docking into the low affinity binding site. The center of the docking grid was defined by the center of the bound ligands as described in the original PDB entry and the volume of the grid was set to 10 Å^3. No further modifications were applied to the default settings (no scaling factor for the vdW radii of nonpolar protein atoms, 0.8 scaling for nonpolar ligand atoms). The GlideScore scoring function was used to select up to 30 poses for each ligand.

Poses obtained from Glide were grouped into clusters of poses within 2 Å using the simple cluster subroutine. A representative structure from each cluster was output in pdb format. Schematic diagrams of protein−ligand interactions were produced using Ligplot.[24] Residues involved in interactions were scored based on occurrences in each cluster with weighting taking into account the number of poses which form each cluster.

Results

Stoichiometry of ANS Binding. Binding curves were obtained by measuring the increase in fluorescence on titration of L-FABP with ANS (Figure 2A). The data were fit to both one-site and two-site binding models. Comparisons of the two models indicate a statistically better fit to the two-site binding hyperbola (Figure 2B) when compared with the one-site binding hyperbola ($p < 0.5$). Specific dissociation constants of 1.1 and 12 μM were obtained for the high affinity and low affinity binding sites, respectively. The fluorescence enhancement observed on ANS binding is consistent with the probe being located within the nonpolar region of the β-barrel.[25] Contributions to overall fluorescence were calculated to be 40.2% and 59.8% for the high and low affinity sites, respectively. This fluorescence enhancement was used to discriminate between binding at the high and low affinity sites in the displacement assays. Further analysis of the binding data (eq 3), determined that the Hill coefficient for ANS binding was 1.1, which is consistent with a noncooperative binding mode of two ANS molecules. This noncooperativity is further supported by the biphasic Scatchard plot (Figure 2B inset).

Binding of Drugs. Competition experiments were performed to investigate the binding of a structurally diverse range of lipophilic drugs (Figure 3) to L-FABP. Displacement of ANS from the binding cavity was measured as the reduction in the fluorescence signal of bound ANS on titrating increasing amounts of competing ligand. The assay was validated via displacement of ANS by oleic acid (Figure 4A). Analysis of the data indicated that oleic acid bound at two sites on L-FABP with K_d values of 0.18 and 2.9 μM, respectively (Table 1). Values obtained for oleate and ANS are in close agreement with published data (K_d values for oleate binding determined by calorimetry were reported as 0.2 and 0.9 μM, respectively,[26] and ANS has previously been reported to bind to human L-FABP with a $K_d = 2$ μM[27]), demonstrating the validity of the ANS displacement assay and the competitive displacement analysis techniques.

The same approach was used to determine the affinity of the different drugs for L-FABP. By way of example, the change in fluorescence on titration with ketorolac, diazepam, and clofibrate are presented in Figure 4 parts B−D. Displacement data were analyzed to obtain K_i values for the various ligands. The values obtained are presented in Table 1. The data obtained for diazepam and clofibrate resulted in a truncation of the titration profile (Figure 4C,D), as the solubility limit of the compounds was reached before the titration was complete. A similar effect

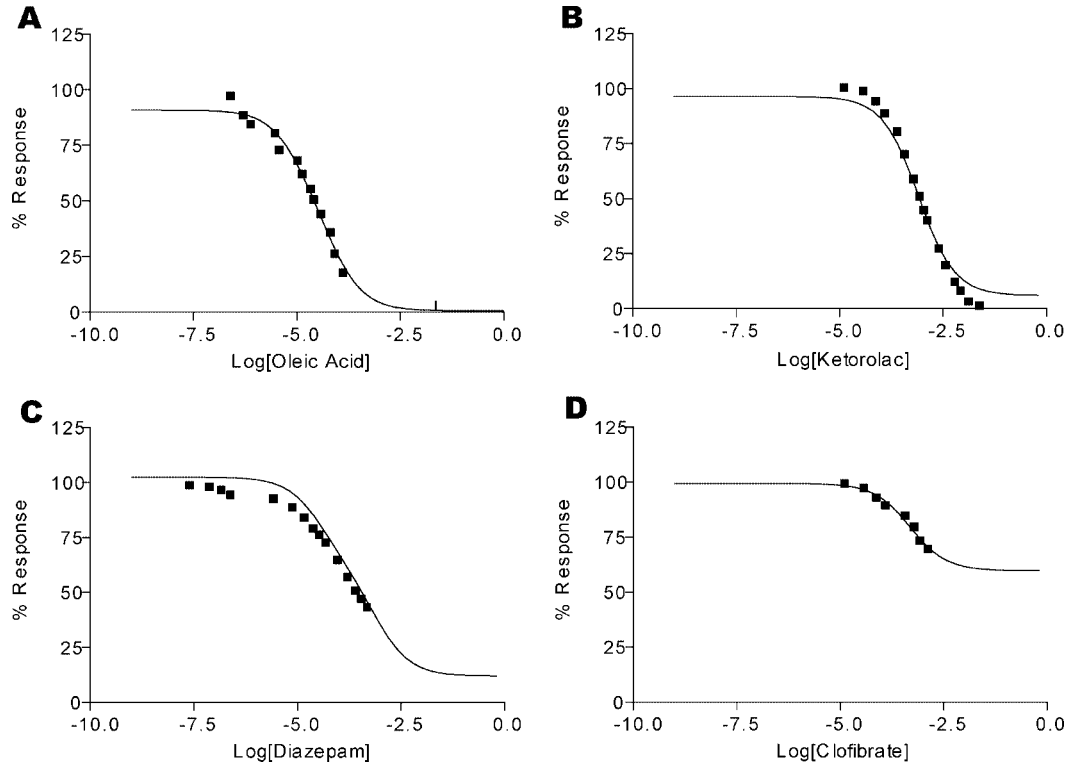

Figure 4. Displacement of ANS from L-FABP by oleic acid (A), ketorolac (B), diazepam (C), and clofibrate (D). L-FABP (1 μM in buffer C) saturated with 70 μM ANS was titrated against competing drugs. Solid lines represent the optimal curve fitting to either a one-site or two-site competition model.

Table 1. Binding Affinity of L-FABP for Various Lipophilic Drugs Determined Fluorimetrically by Displacement of ANS[a]

ligand	K_{i1} (μM)	K_{i2} (μM)	*c* Log *D* $_{pH\ 5.5}$	*c* Log *P*
oleate	0.18 ± 0.016	2.9 ± 0.033	6.9	7.7
ANS	1.1 ± 0.08	12 ± 1.3	−0.22	3.28
atenolol	717 ± 100		−2.90	0.1
nadolol	2310 ± 300		−1.71	1.29
progesterone	0.027 ± 0.0011		4.04	4.04
dexamethasone	22.1 ± 1.5	41.3 ± 3.7	1.87	1.87
prednisolone	2.66 ± 0.23	101 ± 6	1.49	1.49
indoprofen	1.27 ± 0.16	161 ± 40	1.63	2.77
ibuprofen	47.6 ± 9.8	448 ± 39	2.60	3.72
meclofenamic acid	0.379 ± 0.005	0.256 ± 0.012	4.78	6.67
flurbiprofen	1.18 ± 0.12	222 ± 23	2.74	4.12
diclofenac	3.22 ± 0.083	35.4 ± 1.9	2.72	4.06
ketorolac	11.6 ± 0.6	119 ± 5	1.01	2.08
aspirin	348 ± 9	3780 ± 60	−0.80	1.19
bezafibrate		44.4 ± 5.8	1.26	3.46
clofibrate	6.92 ± 0.73		3.32	3.32
gemfibrozil	1.86 ± 0.27	179 ± 22	3.57	4.39
fenofibrate	0.024 ± 0.004	0.405 ± 0.125	4.8	4.80
fenofibric acid	0.334 ± 0.072	27.5 ± 3.7	1.46	3.86
diazepam	0.531 ± 0.058	115 ± 8	2.96	2.96
lorazepam	12.9 ± 0.8	140 ± 7	2.47	2.47

[a] Calculated partition coefficients *c* Log *D* data at pH 5.5 and *c* Log *P* are also tabulated. In all fluorescence assays $n = 3$. Calculated effective partition coefficient (*c* Log *D*) at pH 5.5 calculated using Advance Chemistry Development software v6.00 (ACD/Labs, Toronto, Canada).

was seen for several of the more poorly water-soluble species. However, in most cases, the data available was sufficient to extrapolate for analysis. In the majority of cases, the displacement data were best fit by two-site competition, suggesting that these drugs bound at both sites in L-FABP as exemplified by diazepam (Figure 4C). However, a limited number of drugs, including clofibrate, atenolol, progesterone, and bezafibrate, were better fit by a one-site competition model. The drugs that were found to only bind to one site were then fitted to one-site competition models to compare the fits for binding in the high affinity site or low affinity site (based on the degree of reduction in fluorescence). With the exception of bezafibrate, the best fits of the data were obtained for competitive displacement of ANS from the higher affinity site. However, the data obtained should be viewed with the caveat that the titration data for all of the drugs that were nominally identified as binding to a single site was truncated due to poor solubility in the assay buffer. For drugs with high solubility such as nadolol and aspirin, only one binding site was identified before reaching the DMSO limitations of the assay. It is possible therefore that the drugs with low water solubility also exhibit two-site binding, but that binding to the second site could not be determined due to the solubility limitations.

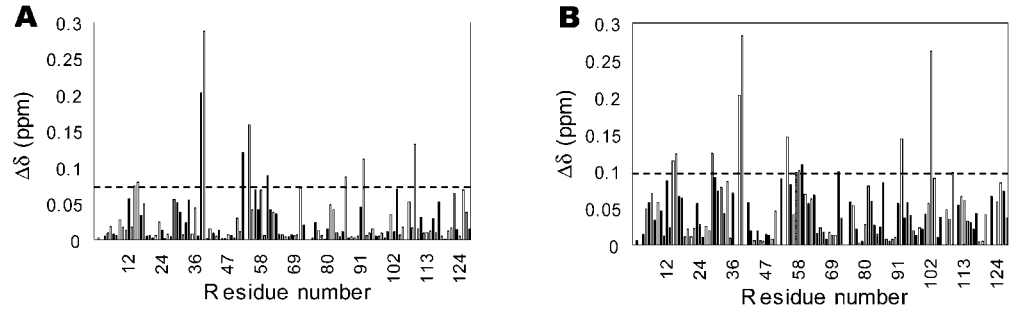

Figure 5. ^{15}N-HSQC titration data for the addition of ketorolac to ^{15}N-labelled L-FABP. Plot of weighted average chemical shift change vs residue number for L-FABP, following the addition of 50 μM (A) or 500 μM (B) of ketorolac. The dotted line represents the mean chemical shift change + one standard deviation.

The inhibition coefficients for the tested drugs and their apparent octanol−water partition coefficients (Log $D_{5.5}$), calculated under the experimental conditions (pH 5.5), are documented in Table 1. In general, drugs with the highest Log *D* showed the greatest binding affinity for L-FABP. Drugs of lower Log *D* showed higher K_i values, indicative of the preferential binding of poorly water soluble species in the hydrophobic core of L-FABP. However, drugs with similar Log *D* did display differences in K_i, suggesting that binding is mediated via specific interactions between L-FABP and the respective drugs and is not dictated by lipophilicity alone. This is exemplified by dexamethasone and prednisolone, which differ structurally only by the substitution of a hydrogen for a fluorine and the removal of a methyl, but where these structural differences result in 10-fold higher binding affinity for prednisolone compared to dexamethasone.

Mapping the Binding Surfaces by ^{1}H−^{15}N HSQC Chemical Shift Perturbation. To probe the binding characteristics of L-FABP, a series of NMR chemical shift perturbation studies were carried out, monitoring changes in the ^{1}H−^{15}N HSQC spectrum of ^{15}N-labeled L-FABP upon the addition of test compounds. Assignments for L-FABP were obtained using standard triple-resonance methods.[28] Test compounds included oleic acid (as an endogenous ligand), ANS (to validate the fluorescence data), ketorolac (found to displace at both binding sites), ibuprofen (as an example of extrapolated data indicating two-site binding), or progesterone (extrapolated data indicating single-site binding), which were titrated into a labeled sample of L-FABP from either buffer C or DMSO. The results of the titrations for each compound were compared at two concentrations. At the lower concentration, the higher affinity site was expected to be significantly populated, whereas at the higher concentration, L-FABP was approaching saturation based on the K_d values calculated in the fluorescence experiments. Analyses of the changes in the amide chemical shifts in the ^{1}H−^{15}N HSQC spectra provide a means by which the location of the ligand binding site of L-FABP may be identified. Weighted chemical shift changes upon addition of ketorolac are shown as an example in Figure 5. Significant changes in chemical shift were defined as more than one standard deviation greater than the mean change.

The results of the titrations were mapped onto the structure of L-FABP as shown in Figure 6. As unlabeled oleic acid was titrated into ^{15}N-labeled L-FABP to the lower concentration (50 μM), it was observed that a subset of peaks, as indicated by the red and pink regions in Figure 6A, showed the most significant changes in chemical shift. These residues were consistent with residues located in the vicinity of the high affinity binding site of the crystal structure. When oleic acid was titrated into ^{15}N-labeled L-FABP to the higher concentration (200 μM), an additional group of residues were perturbed (indicated by the blue regions in Figure 6A), which were located at positions consistent with the location of the low affinity binding site, including residues in βA, βB, βC, βE, and βF, as well as αI and αII. Thus, the majority of significantly perturbed residues are localized within the binding sites for oleic acid, and perturbations observed at different ligand concentrations were able to discriminate the high and low affinity binding sites on L-FABP.

The residues that were perturbed in the presence of the lower concentration (50 μM) of ANS were localized within the β-barrel (Figure 6C) and located in a similar region of L-FABP as those residues involved in the binding of oleate at the high affinity site.[18] Additional residues that were perturbed at the higher concentration (200 μM) of ANS were localized around the helical cap region, in the vicinity of the low affinity binding site for oleate in the crystal structure.[18] These results indicate that ANS occupies similar binding sites to oleic acid and is consistent with the data obtained from the fluorescence displacement assay.

On titration of ketorolac into ^{15}N-labeled L-FABP, the residues perturbed at the lower concentration (50 μM) were again located at the base of the barrel structure (Figure 6D). Of significant note is the perturbation of Ser^{39}, which is involved in the hydrogen bonding network of oleate in the crystal structure and suggests a potentially interaction with the carboxylate of ketorolac. Other perturbed backbone amides include Val^{92}, Leu^{71}, and Val^{38}, which are adjacent to the position of oleate bound in the high affinity site of the crystal structure. At the higher concentration (500 μM), significant perturbations were observed for Lys^{57}, Ile^{29}, and Tyr^{54}. These residues form part of the low affinity binding site for oleic acid. At the higher concentration of ketorolac, several residues within the helical cap were also perturbed, consistent with binding at the low affinity site of L-FABP.

Titration of ibuprofen into ^{15}N-labeled L-FABP resulted in two subsets of perturbed residues. Residues perturbed at the lower concentration (100 μM) were located over the barrel structure, whereas residues perturbed at the higher concentration (900 μM) spread across the barrel structure and the α-helical caps (Figure 6E). This suggested that the low affinity binding site for ibuprofen was at the cap region and supported the two-site binding model derived from the extrapolated fluorescence data.

When progesterone was titrated into ^{15}N-labeled L-FABP, significant perturbation of resonances for residues at the α-helical cap was seen even at the lower concentration (50 μM) (Figure 6F). These changes were more pronounced at the higher concentration (200 μM), however, the perturbed residues were similar at both progesterone concentrations. At the higher

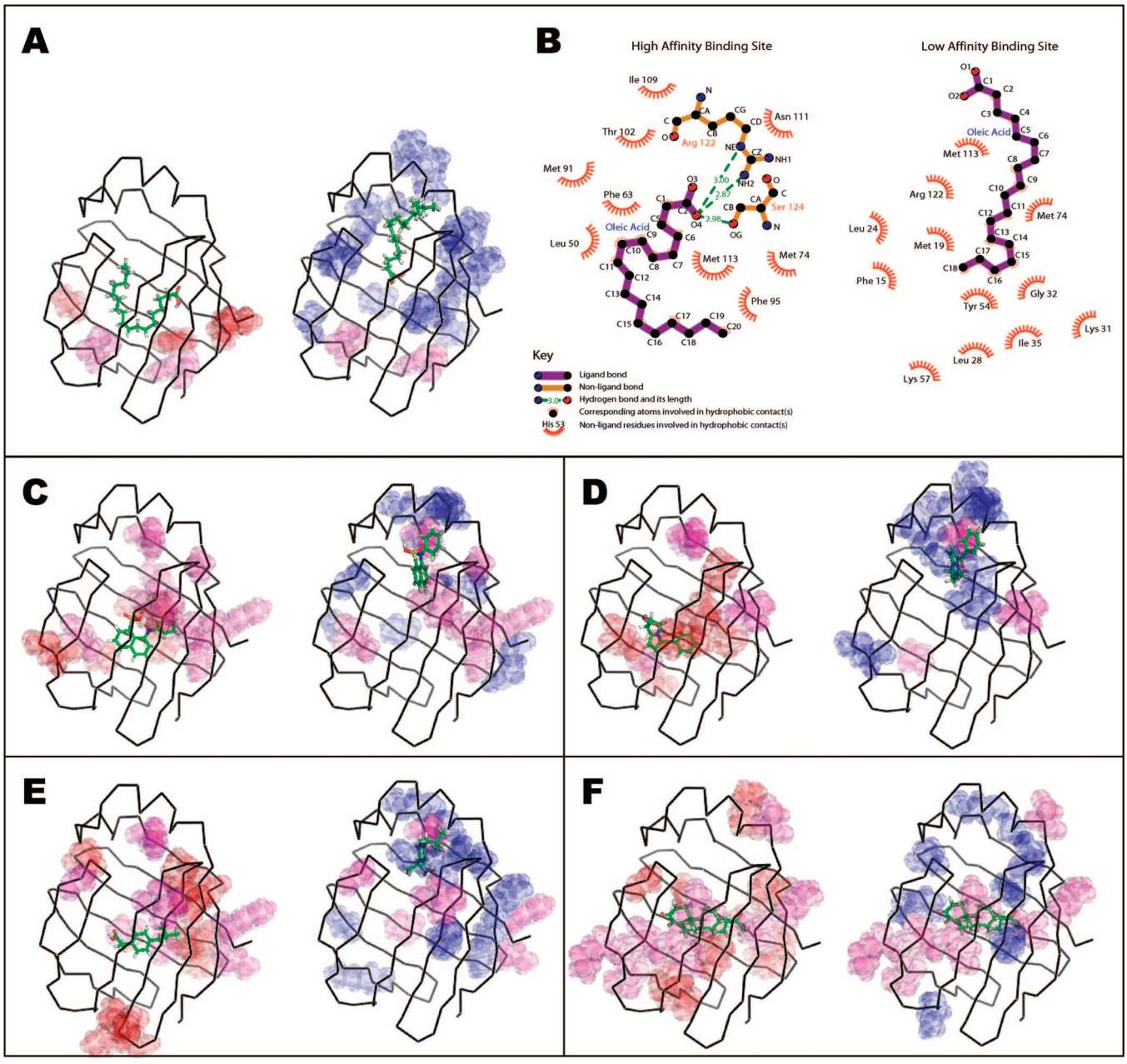

Figure 6. Ligands are shown in wire representation in the optimal docking solutions. Amides of residues which were significantly perturbed are shown in red (left structure) and blue (right structure) spheres for the low and high concentrations used in the titrations. At the lower concentration in each titration, the high affinity site is more significantly populated. At the higher concentration, the protein is approaching saturation. Residues perturbed at both these concentrations are shown in pink. Ligands shown are oleic acid (A), ANS (C), ketorolac (D), ibuprofen (E), and progesterone (F). Ligplot representation of optimal oleic acid binding site is also shown in (B).

concentration of progesterone, the perturbations differed in the extent rather than location. The data were consistent with the fluorescence data that found progesterone only bound to a single binding site. While the majority of perturbed resonances are more consistent with binding to the high affinity site, perturbation of the helical cap residues may reflect accommodation of the bulkier ligand.

Molecular Docking. Molecular docking models were generated and compared with the results of the NMR titration studies. The modeling approach was first validated by docking two oleate molecules into the binding cavity of L-FABP crystal structure. The two oleates were docked into the structure in a stepwise manner. In all docking clusters, the first oleate was found to form a salt bridge between the carboxylate headgroup and Arg^{122}, consistent with the crystal structure. An example of the oleic acid docking cluster is seen in Figure 6A, with the Ligplot representation shown in 6B. Other interactions occurring frequently in the clusters include those with Ser^{124}, which is involved in the extensive hydrogen bonding network found in the crystal structure, as well as Met^{113}, $Thr^{102,}$ and Ser^{39}, which are also in contact with the oleate in the high affinity binding site. For the second binding site, the first oleate was retained in the L-FABP binding cavity and docking solutions obtained for the second molecule. In all docking clusters for the second site, interactions were seen with one or more of Lys^{31}, $Ser^{56,}$ and Tyr^{54}. This is consistent with residues located near the carboxylate headgroup of the second oleate in the crystal structure. Other residues, which were consistently involved in interactions with the second oleic acid in the docking solutions, are residues residing in contact with hydrophobic tail of the second oleate

in the crystal structure, including Gly[32], Ile[35], Arg[122], and Lys[57]. Thus the docking approach employed was able to regenerate the binding modes observed in the crystal structure of the complex (Figure 6A). The same procedure was used to dock the drugs and ANS into the binding cavity of L-FABP.

ANS was seen to have three clusters of poses within the high affinity binding site with slight differences in ANS orientations. The main contacts identified in these clusters were with Leu[50], Thr[102], Ser[39], Phe[63,] and Met[91], which are residues located at the base of the binding cavity of L-FABP. The docking of the second ANS molecule resulted in a single cluster of poses, with contacts being made to Phe[15], Leu[24], and Lys[31], all of which are in the α-helical cap region, as well as Ile[52], Tyr[54], Lys[57], Ile[59], and Met[74], which are residues in the vicinity of the hairpin turns of βC, βD, and βE, which form part of the portal. The docked poses were consistent with the NMR data, with the most significant perturbations being observed for residues adjacent to the sites of binding.

Ibuprofen displayed two clusters of poses at the high affinity binding site, with hydrogen bonding occurring at Ser[100], Arg[122], or Ser[124]. Significant contacts seen were Ser[39], Leu[50], and Ile[109], located at the bottom of the binding cavity. A further three clusters were seen at the low affinity binding site, showing main hydrogen bonding contacts to be Tyr[120] and Arg[122]. The most frequently occurring contacts were Met[19], Gly[32], Tyr[54], and Lys[57], which are all residues within the α-helices, as well as residues at the hairpin turn between βC and βD. Again, these poses were consistent with the perturbations observed in the NMR data.

Ketorolac displayed two clusters of poses at the high affinity binding site and five clusters at the low affinity binding site. Residues most often involved in hydrogen bonding at the high affinity site were Thr[102] and Glu[72], whereas for the low affinity binding site, potential hydrogen bonding residues were Asn[111], Tyr[120], Arg[122], Leu[28], and Tyr[54]. The main contacts of the high affinity binding site were found to be Leu[50], Phe[63], and Val[83], located at the base of the β-barrel. The most notable contacts of the low affinity binding site were Met[74] and Gly[32], in the cap region.

Progesterone was found to only bind to the high affinity binding site forming a hydrogen bond with Ser[124]. Sites of contact were spread across the central region of the barrel cavity at Leu[50], Ile[51], Phe[95], Thr[102], Ile[109], Asn[111], Met[113], and Arg[122]. This docking solution was distinct from the docking solutions for the other drugs, as it was situated across both the high and low affinity binding sites. This is consistent with the NMR perturbation data, which showed perturbation across the β-barrel structure, as well as the fluorescence binding data, which indicated only one binding site.

Taken together, the combined spectroscopic and docking data suggest that most of the drugs studied can bind to both fatty acid binding sites of L-FABP. There are a variety of different modes of binding, which can be accommodated with the binding cavity which allows L-FABP to bind to a diverse range of lipophilic drug molecules.

Discussion

For most orally administered drugs, the principle sites of absorption are the absorptive cells that line the intestines (enterocytes). An increasing body of work has led to the identification of numerous transporters that facilitate movement across the basal and apical membranes of these cells. However, relatively little is known about the processes by which drugs transverse the aqueous cytosol. For endogenous molecules such as fatty acids, which have extremely poor water solubility, cytosolic fatty acid binding proteins (FABPs) are known to enhance their aqueous solubility and facilitate their intracellular transport.[29] Within the enterocyte there are two FABPs, which are thought to associate with fatty acids via different mechanisms. It is believed I-FABP collides with the membrane from which FAs are extracted,[30] whereas L-FABP is thought to associate with FA after they have diffused out of the membrane into the cytosol.[30] Therefore, the presence of both I-FABP and L-FABP contribute to absorption and cellular disposition of FA.

Because of the abundance of these proteins, at levels as high as 8% of total soluble cytosolic protein,[31] it has been suggested that they may play a role in the transport of not only endogenous fatty acids but also exogenous lipophilic species. It has been demonstrated that the large binding cavity of L-FABP (610 Å^2)[2] facilitates accommodation of a range of diverse ligands including endogenous lipophilic species such as heme and prostaglandins. L-FABP has also been shown to bind to some lipophilic drugs,[9,32] although to date there has been no reports of the broader binding specificity of L-FABP for lipophilic drugs and the mode of binding to L-FABP has not been characterized. As such, we report here the binding of L-FABP to a diverse range of exogenous lipophilic species.

In the current studies, a range of structurally diverse drugs have been shown to bind L-FABP using a combination of fluorescence displacement assays and $^1H-^{15}N$ HSQC NMR chemical shift perturbation experiments. The ANS displacement data indicated that most of the drugs investigated were bound at both high affinity and low affinity sites of L-FABP. This was confirmed in the NMR perturbation experiments, where for most of the test compounds, two localized regions of perturbation were identified, consistent with the presence of two binding sites.

Although there have been few studies describing the structural basis of the interaction of L-FABPs with exogenous ligands, it has previously been suggested that it is the low affinity site (where L-FABP binds its second FA predominantly via hydrophobic interactions) that is likely to be the more promiscuous binding site and capable of interacting with a variety of lipophilic species.[29] However, for the majority of the compounds tested here, binding was observed at two sites. The binding sites were observed in similar locations to those found for oleic acid in the crystal structure with L-FABP. However, a striking feature of the interaction of L-FABP with lipophilic drugs is that our data suggest that a carboxylate is not an absolute requirement for binding at the internal site of L-FABP. The FA in the high affinity site of L-FABP is stabilized via an ionic interaction with Arg[122], and it has been hypothesized that this interaction is necessary for high affinity binding.[18] However, in our data set, we observed, for example that fenofibrate, which is an ester, binds with 10-fold greater affinity than its carboxylate counterpart, fenofibric acid at the higher affinity site, and that both compounds exhibit two-site binding. Across the series of fibrates that were tested, two are esters and three are carboxylates. All were found to bind L-FABP, with fenofibrate having the highest affinity. Thus it appears that a terminal carboxylate is not required for high affinity binding to L-FABP in this series. In addition, several other drug molecules lacking a carboxylate group were found to bind to L-FABP. For example progesterone, was found to bind with reasonable affinity, although it appeared to bind at only a single site, whereas the benzodiazepines (diazepam and lorazepam) each bound at two sites on L-FABP. Thus, it appears that there are several modes of binding that allow a structurally diverse range of ligands to bind to L-FABP. The importance of the hydrophobic interactions in dictating the

binding specificity of L-FABP is consistent with previous mutational data, which found that the mutation of Arg^{122}-Gln had little effect on the affinity of binding of oleic acid.[34]

From the current data, it can be inferred that L-FABP binds preferentially to drugs with poor water solubility. This is consistent with results obtained by other groups, which have demonstrated that there is an inverse relationship between binding affinity for L-FABP and aqueous solubility for both fatty acids and peroxisome proliferators.[9,33] Although most of the drugs tested were found to bind L-FABP with generally lower affinities than FA, their interaction with L-FABP may well be significant because an analogous situation arises in the bloodstream, where many drugs bind albumin (HSA) with a relatively low affinity ($K_d > 10\ \mu M$) but where the proportion of the total drug in plasma that is bound to HSA is often significant both from a physiological and clinical perspective.[35]

Comparison of the binding specificity of L-FABP with that previously reported for drug binding to I-FABP indicates some similarities. In general, those drugs that bound to I-FABP were also found to bind to L-FABP. Lipophilic carboxylic acids are highly represented across the compounds that bind to both proteins, as might be expected. However, the majority of drugs tested bound with higher affinity to L-FABP in comparison to I-FABP. This observation holds true both for carboxylic acids, e.g., flurbiprofen ($K_i = 26\ \mu M$ for I-FABP as determined by ANS displacement), meclofenamic acid ($K_i = 8.9\ \mu M$ for I-FABP as determined by ANS displacement), fenofibric acid ($K_i = 1.0\ \mu M$ for I-FABP as determined by ANS displacement), as well as for uncharged compounds, e.g., progesterone ($K_i = 20\ \mu M$ for I-FABP as determined by ANS displacement).[15] Of the drugs tested, only bezafibrate was found to bind to I-FABP with higher affinity, albeit under different buffer conditions ($K_i = 33\ \mu M$ for I-FABP as determined by ANS displacement). Furthermore, L-FABP appears to be capable of binding to a broader range of lipophilic drug molecules than I-FABP. For example, several compounds which bound to I-FABP with K_i values ≥ 1 mM determined by ANS displacement, including dexamethasone, diazepam, lorazepam, and ketorolac, were found to bind to L-FABP with μM or sub-μM affinities. The similarity between rat and human L-FABP, which share 82% sequence identity, suggests that the binding specificities observed for the rat protein may be indicative of those of the human protein.

We have recently demonstrated that I-FABP is capable of increasing the transmembrane flux of lipophilic drugs that bind with low micromolar K_d. The current data, therefore, suggest that lipophilic drug binding to L-FABP may influence membrane permeability, and indicates a potential role for L-FABP in cellular drug disposition.

Acknowledgment. We acknowledge E. Yuriev and D. K. Chalmers for assistance with docking studies. This work was supported by grants from the Australian Research Council (DP0342458, DP0664069). S.C. gratefully acknowledges financial support provided by an Australian Postgraduate Scholarship. T.V. is the recipient of a Peter Doherty Fellowship (384300) from the National Health and Medical Research Council of Australia.

References

(1) Haunerland, N. H.; Spener, F. Fatty acid-binding proteins: insights from genetic manipulations. *Prog. Lipid Res.* **2004**, *43* (4), 328–349.

(2) Thompson, J.; Ory, J.; Reese-Wagoner, A.; Banaszak, L. The liver fatty acid binding protein: comparison of cavity properties of intracellular lipid-binding proteins. *Mol. Cell. Biochem.* **1999**, *192* (1−2), 9–16.

(3) Arighi, C. N.; Rossi, J. P.; Delfino, J. M. Temperature-induced conformational switch in intestinal fatty acid binding protein (IFABP) revealing an alternative mode for ligand binding. *Biochemistry* **2003**, *42* (24), 7539–7551.

(4) Hanhoff, T.; Lucke, C.; Spener, F. Insights into binding of fatty acids by fatty acid binding proteins. *Mol. Cell. Biochem.* **2002**, *239* (1−2), 45–54.

(5) Winter, N. S.; Gordon, J. I.; Banaszak, L. J. Characterization of crystalline rat liver fatty acid binding protein produced in *Escherichia coli*. *J. Biol. Chem.* **1990**, *265* (19), 10955–10958.

(6) Gordon, J. I.; Alpers, D. H.; Ockner, R. K.; Strauss, A. W. The nucleotide sequence of rat liver fatty acid binding protein mRNA. *J. Biol. Chem.* **1983**, *258* (5), 3356–3363.

(7) Vassileva, G.; Huwyler, L.; Poirier, K.; Agellon, L. B.; Toth, M. J. The intestinal fatty acid binding protein is not essential for dietary fat absorption in mice. *FASEB J.* **2000**, *14* (13), 2040–2046.

(8) Thompson, J.; Reese-Wagoner, A.; Banaszak, L. Liver fatty acid binding protein: species variation and the accommodation of different ligands. *Biochim. Biophys. Acta* **1999**, *1441* (2−3), 117–130.

(9) Wolfrum, C.; Borchers, T.; Sacchettini, J. C.; Spener, F. Binding of fatty acids and peroxisome proliferators to orthologous fatty acid binding proteins from human, murine, and bovine liver. *Biochemistry* **2000**, *39* (6), 1469–1474.

(10) Weisiger, R. A. Cytosolic fatty acid binding proteins catalyze two distinct steps in intracellular transport of their ligands. *Mol. Cell. Biochem.* **2002**, *239* (1−2), 35–43.

(11) Glatz, J. F.; van der Vusse, G. J. Cellular fatty acid-binding proteins: their function and physiological significance. *Prog. Lipid Res.* **1996**, *35* (3), 243–282.

(12) Bass, N. M.; Manning, J. A. Tissue expression of three structurally different fatty acid binding proteins from rat heart muscle, liver, and intestine. *Biochem. Biophys. Res. Commun.* **1986**, *137* (3), 929–935.

(13) Velkov, T.; Chuang, S.; Wielens, J.; Sakellaris, H.; Charman, W. N.; Porter, C. J.; Scanlon, M. J. The interaction of lipophilic drugs with intestinal fatty acid binding protein. *J. Biol. Chem.* **2005**, *280* (18), 8.

(14) Kanda, T.; Ono, T.; Matsubara, Y.; Muto, T. Possible role of rat fatty acid-binding proteins in the intestine as carriers of phenol and phthalate derivatives. *Biochem. Biophys. Res. Commun.* **1990**, *168* (3), 1053–1058.

(15) Velkov, T.; Horne, J.; Laguerre, A.; Jones, E.; Scanlon, M. J.; Porter, C. J. Examination of the role of intestinal fatty acid-binding protein in drug absorption using a parallel artificial membrane permeability assay. *Chem. Biol.* **2007**, *14* (4), 453–465.

(16) Cistola, D. P.; Sacchettini, J. C.; Banaszak, L. J.; Walsh, M. T.; Gordon, J. I. Fatty acid interactions with rat intestinal and liver fatty acid-binding proteins expressed in Escherichia coli. A comparative ^{13}C NMR study. *J. Biol. Chem.* **1989**, *264* (5), 2700–2710.

(17) Hamilton, J. A. Fatty acid interactions with proteins: what X-ray crystal and NMR solution structures tell us. *Prog. Lipid Res.* **2004**, *43* (3), 177–199.

(18) Thompson, J.; Winter, N.; Terwey, D.; Bratt, J.; Banaszak, L. The crystal structure of the liver fatty acid-binding protein. A complex with two bound oleates. *J. Biol. Chem.* **1997**, *272* (11), 7140–7150.

(19) Velkov, T.; Chuang, S.; Prankerd, R.; Sakellaris, H.; Porter, C. J.; Scanlon, M. J. An improved method for the purification of rat liver-type fatty acid binding protein from *Escherichia coli*. *Protein Expression Purif.* **2005**, *44* (1), 23–31.

(20) Delaglio, F.; Grzesiek, S.; Vuister, G. W.; Zhu, G.; Pfeifer, J.; Bax, A. NMRPipe: a multidimensional spectral processing system based on UNIX pipes. *J. Biomol. NMR* **1995**, *6* (3), 277–293.

(21) Goddard, T. D.; Kneller, D. G. *SPARKY 3*; University of California: San Francisco, 2001.

(22) Ayed, A.; Mulder, F. A.; Yi, G. S.; Lu, Y.; Kay, L. E.; Arrowsmith, C. H. Latent and active p53 are identical in conformation. *Nat. Struct. Biol.* **2001**, *8* (9), 756–760.

(23) Friesner, R. A.; Banks, J. L.; Murphy, R. B.; Halgren, T. A.; Klicic, J. J.; Mainz, D. T.; Repasky, M. P.; Knoll, E. H.; Shelley, M.; Perry, J. K.; Shaw, D. E.; Francis, P.; Shenkin, P. S. Glide: a new approach for rapid, accurate docking and scoring. 1. Method and assessment of docking accuracy. *J. Med. Chem.* **2004**, *47* (7), 1739–1749.

(24) Wallace, A. C.; Laskowski, R. A.; Thornton, J. M. LIGPLOT: a program to generate schematic diagrams of protein−ligand interactions. *Protein Eng.* **1995**, *8* (2), 127–134.

(25) Kane, C. D.; Bernlohr, D. A. A simple assay for intracellular lipid-binding proteins using displacement of 1-anilinonaphthalene 8-sulfonic acid. *Anal. Biochem.* **1996**, *233* (2), 197–204.

(26) Miller, K. R.; Cistola, D. P. Titration calorimetry as a binding assay for lipid-binding proteins. *Mol. Cell. Biochem.* **1993**, *123*, 29–37.

(27) Veerkamp, J. H.; van Moerkerk, H. T.; Prinsen, C. F.; van Kuppevelt, T. H. Structural and functional studies on different human FABP types. *Mol. Cell. Biochem.* **1999**, *192* (1−2), 137–142.

(28) Grzesiek, S.; Bax, A. Improved 3D triple-resonance NMR techniques applied to a 31 kDa protein. *J. Magn. Reson.* **1992**, *96*, 432–440.

(29) Zimmerman, A. W.; Veerkamp, J. H. New insights into the structure and function of fatty acid-binding proteins. *Cell. Mol. Life Sci.* **2002**, *59* (7), 1096–1116.
(30) Hsu, K. T.; Storch, J. Fatty acid transfer from liver and intestinal fatty acid-binding proteins to membranes occurs by different mechanisms. *J. Biol. Chem.* **1996**, *271* (23), 13317–13323.
(31) Lowe, J. B.; Sacchettini, J. C.; Laposata, M.; McQuillan, J. J.; Gordon, J. I. Expression of rat intestinal fatty acid-binding protein in *Escherichia coli*. Purification and comparison of ligand binding characteristics with that of *Escherichia coli*-derived rat liver fatty acid-binding protein. *J. Biol. Chem.* **1987**, *262* (12), 5931–5937.
(32) Wolfrum, C.; Buhlmann, C.; Rolf, B.; Borchers, T.; Spener, F. Variation of liver-type fatty acid binding protein content in the human hepatoma cell line HepG2 by peroxisome proliferators and antisense RNA affects the rate of fatty acid uptake. *Biochim. Biophys. Acta* **1999**, *1437* (2), 194–201.
(33) Richieri, G. V.; Ogata, R. T.; Kleinfeld, A. M. Equilibrium constants for the binding of fatty acids with fatty acid-binding proteins from adipocyte, intestine, heart, and liver measured with the fluorescent probe ADIFAB. *J. Biol. Chem.* **1994**, *269* (39), 23918–23930.
(34) Thumser, A. E.; Voysey, J.; Wilton, D. C. Mutations of recombinant rat liver fatty acid-binding protein at residues 102 and 122 alter its structural integrity and affinity for physiological ligands. *Biochem. J.* **1996**, *314*, 943–949.
(35) Kock-Weser, J. Pharmacokinetics of antiarrhythmic drugs. *Cardiovasc. Clin.* **1975**, *7* (2), 191–202.

JM701192W